HHS Public Access

Author manuscript

Biochemistry. Author manuscript; available in PMC 2018 January 02.

Published in final edited form as:

Biochemistry. 2016 July 19; 55(28): 3995–4002. doi:10.1021/acs.biochem.6b00467.

ATP IS AN ALLOSTERIC INHIBITOR OF COXSACKIEVIRUS B3 POLYMERASE

Jonathan P. Karr and **Olve B. Peersen***

Department of Biochemistry and Molecular Biology, Colorado State University, Fort Collins, CO 80523, USA

Abstract

The RNA-dependent RNA polymerases from positive strand RNA viruses, such as picornaviruses and flaviviruses, close their active sites for catalysis via a unique NTP-induced conformational change in the palm domain. Combined with a fully pre-positioned templating nucleotide, this mechanism is error-prone and results in a distribution of random mutations in the viral progeny often described as a quasispecies. Here we examined the extent to which non-cognate NTPs competitively inhibit single cycle elongation by coxsackievirus B3 $3D^{pol}$, a polymerase that generates 3–4 mutations per 10 kb of RNA synthesized during viral infection. Using an RNA with a templating guanosine combined with 2-aminopurine fluorescence as a reporter for elongation, we find that the cognate CTP has a K_m of 24 μM and the three non-cognate nucleotides competitively inhibit the reaction with K_{ic} values of 500 μM for GTP, 1300 μM for ATP, and 3000 μM for UTP. Unexpectedly, ATP also acted as an uncompetitive inhibitor with a K_{iu} of 1800 μM, resulting in allosteric modulation of $3D^{pol}$ that slowed the polymerase elongation rate ≈4-fold. ATP uncompetitive inhibition required the β- and γ-phosphates and was significantly diminished in two previously characterized low-fidelity polymerases. This led to further mutational analysis and the identification of a putative allosteric binding site below the NTP entry channel at the interface of conserved motifs A and D, although co-crystallization failed to reveal any density for bound ATP in this pocket. The potential role of an ATP allosteric effect during the virus lifecycle is discussed.

Graphical Abstract

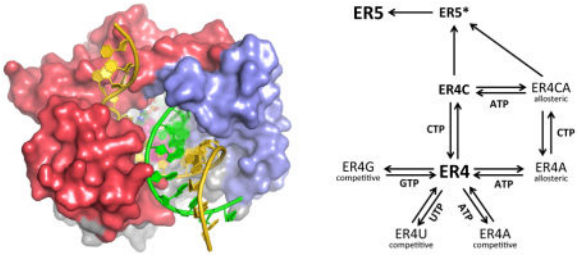

*Corresponding Author: Olve.Peersen@ColoState.edu – Telephone: 970-491-0433.

Author Contributions

JPK carried out the experiments and JPK and OBP wrote the manuscript.

Notes

The authors declare no competing financial interests.

Keywords

Coxsackievirus; Polymerase; Allostery; Mixed Inhibition

Viruses of the family *Picornaviridae* comprise an important class of pathogens that continues to take a major toll on human and animal health across the globe with a large variety of diseases, including the common cold, foot-and-mouth-disease, poliomyelitis, and heart disease.[1,2] Remarkably, such diversity is achieved with small 7.5 to 10 kb genomes[3] and a proteome of only eight mature proteins that exhibit a high level of antigenic conservation across species.[4] Though their adaptability has made picornaviruses difficult to treat and eradicate, the conservation of certain viral proteins provides hope for broad-spectrum antivirals.[5,6] Currently, however, no such antivirals exist, though there have been numerous lead compounds targeting different points in the virus lifecycle, especially through inhibition of nonstructural protein function.[6] One such protein is $3D^{pol}$, the viral RNA-dependent RNA polymerase (RdRP) that performs both negative- and positive-strand RNA synthesis to allow for an exclusively RNA-based virus replication cycle. $3D^{pol}$ shares the characteristic fold of nucleic acid polymerases, described as a cupped right hand with palm, fingers, and thumb domains that form three channels intersecting at the active site: the template entry channel, the NTP entry channel, and the product exit channel. $3D^{pol}$ structures show that the tips of the fingers domain contact the top of the thumb in an interaction that stabilizes the protein structure.[7,8] Notably, the positive-strand RNA virus polymerases close their active sites for catalysis by a unique rearrangement of motif A in the palm domain.[9] These polymerases also have fairly low replication fidelity, resulting in genetically diverse progeny virus populations described as quasi-species that share an overall consensus sequence, but within which individual viral genomes differ at a few random locations.[10]

In the context of a host cell, $3D^{pol}$ must discriminate between all four NTPs as it replicates the viral genome and its fidelity is dictated by the efficiency with which it incorporates the cognate nucleotide over non-cognate nucleotides. This efficiency can be quantitated as the quotient of two kinetic parameters, the rate of nucleotide incorporation (k_{pol}) over the Michaelis constant (K_m) for the nucleotide. The k_{pol} term encompasses both the chemical catalysis and translocation steps and thus represents the successful incorporation of a nucleotide into the nascent chain because the viral RdRPs do not have any proofreading mechanisms that could excise an incorrect nucleotide. The relative affinities of the enzyme-RNA complex for the respective nucleotides are therefore a significant contributor to fidelity, and, along with corresponding rates of incorporation, dictate the rates of misincorporation and thus which misincorporations are more likely.[11] Indeed, the competitive inhibitor constant (K_{ic}), which describes a complex's affinity for the inhibitor species, is equivalent to K_m for that species as an alternate substrate.[12] Hence, a mutant that differentially affects the polymerase's affinities and incorporation rates for different nucleotides has the potential to modulate fidelity in terms of the types of mutations that are made and the relative frequencies at which they occur. Measurement of competitive inhibition constants could therefore be another *in vitro* tool to provide insights into RdRP fidelity determinants.

Previous studies found that conformational dynamics in the $3D^{pol}$ palm domain are principally responsible for structuring the active site for catalysis,[9] which inspired the design of a series of mutations in Coxsackievirus B3 (CVB3) $3D^{pol}$ to alter replication fidelity and attenuate viral replication.[13,14] Virology studies showed that several palm domain mutants were genetically stable and resulted in mutator phenotype viruses, and that *in vivo* mutation rates correlated with the polymerases' ability to discriminate between 2′-deoxy-CTP (dCTP) and CTP *in vitro*. Of these, the I230F and F232Y mutants in motif A had the most dramatic phenotypes and lowest discrimination factors. These two mutations did not significantly alter K_m for CTP, which is to say that they did not have a direct effect on nucleotide recognition. Rather, they increased the maximum elongation rate by >20%, suggesting that active site closure rather than nucleotide binding is the fidelity checkpoint these mutants bypass. Residues 230 and 232 are on the side of the motif A beta-strand facing away from the active site and the mutations appear to decrease polymerase fidelity by disrupting motif A dynamics during active site closure, thereby impacting catalytic efficiency. This provides further evidence that dynamic restructuring of the palm domain is needed for active site closure.

In this work we investigated the effects of non-cognate nucleotides on the rate of CMP incorporation by $3D^{pol}$ using stopped-flow fluorescence to detect the post-catalysis translocation of RNA. As expected, all the non-cognate NTPs exhibit competitive inhibition, but interestingly ATP also has a strong uncompetitive component, indicating it can serve as an allosteric modulator of CVB3 $3D^{pol}$ elongation rates. A mutational analysis suggests this may involve a binding pocket between motifs A and D under the NTP entry channel.

Materials and Methods

Mutagenesis, Protein Expression, Purification

Site-directed mutagenesis was performed using the QuikChange protocol (Agilent Technologies) and confirmed through sequencing by Genewiz, Inc. Protein constructs were expressed and purified as described previously.[15]

Elongation Complex Assembly

Elongation complexes (EC) were made using a self-priming RNA hairpin template containing a single fluorescent 2-aminopurine (2AP) base analog positioned such that catalysis followed by translocation changes 2AP base-stacking, resulting in a significant fluorescence decrease (see Figure 1). ECs were assembled using final concentrations of 10 μM RNA, 30 μM $3D^{pol}$, 112 mM NaCl, 4 mM $MgCl_2$, 2 mM HEPES pH 7, and 5 mM TCEP (tris(2-carboxyethyl)phosphine) reducing agent. ATP and GTP, the first two NTPs need to initiate on the template RNA, were included at 60 μM each and the reaction was incubated for 30 minutes at room temperature to yield a stalled EC with a templating guanosine in the +1 position and the 2AP in the +2 position where it is fully unstacked from neighboring bases and maximally fluorescent. This reaction was then diluted 200-fold in reaction buffer (75 mM NaCl, 4 mM $MgCl_2$, 2 mM HEPES pH 7) and used in stopped-flow fluorescence experiments at a final EC concentration of 12.5 nM in the reaction observation cell.

Stopped-Flow Experiments

All solutions used in stopped-flow experiments were in reaction buffer and all NTP solutions were prepared such that the Mg^{2+} concentration was in 4 mM excess over the final NTP concentration. Elongation reactions were carried out at 30 °C in a Bio-Logic SFM-4000 titrating stopped-flow instrument with an MOS-500 spectrometer. Fluorescence excitation was at 313 nm with a 10 nm bandwidth and emission was detected using a 370/36 nm band pass filter. Total experiment time for an 8-point titration series was 80 seconds.

Graphical data analysis

Rates of individual single nucleotide incorporation experiments were determined by curve fitting in *KaleidaGraph* (Synergy Software, Reading, PA). The fluorescence traces observed in this system (Figure 3A) are best fit to a double exponential plus a linear component, with the amplitude of the first exponential approximately ten times that of the second. Inhibition constants were then calculated using Dixon and Cornish-Bowden linearization plots of the rates.[16,17] The points of intersection were calculated in *Prism 6.0* (GraphPad software, Inc., La Jolla, CA) by performing a global fit in which all the linear fits were constrained to share a common (x,y) coordinate pair that reflects their intersection point.

Kinetic Modeling

To corroborate the graphical analysis, kinetic simulation was performed using the computer program *KinTek Explorer* (KinTek Corp, Snow Shoe, PA).[18,19] KinTek Explorer uses a discrete differential equation solver to simultaneously fit a user-defined model to multiple experimental data, using initial conditions and information about which chemical species are observable to fit rate and non-rate parameters to the given model by minimizing χ^2 across all datasets simultaneously. A major advantage of KinTek Explorer is that it can handle very complicated models and give rigorous error estimates of fitted parameters. Ratios of parameters can also be fixed, allowing for equilibrium constants to be defined without precise knowledge of the on- and off-rates.

The overall model that was used to fit the stopped-flow data is schematized in Figure 2. The center species, ER4, represents the enzyme-RNA complex that has stalled after the initial AAAG nucleotide incorporation steps. At this point, all four NTPs compete for the active site, with CTP-binding being the lone productive pathway. All NTP on-rate constants were assumed to be equivalent at 1 $\mu M^{-1}s^{-1}$ while their off-rates were allowed to vary to fit the dissociation constants. In addition to binding competitively in the active site, ATP can bind to an allosteric site either before or after CTP binds in the active site; this results in an $ER4A_{allosteric}$ complex or a doubly liganded $ER4CA_{allosteric}$ complex that has a slower elongation rate than the native ER4C complex. Catalysis followed by translocation results in an intermediate ER5* species which relaxes to a stalled complex (ER5) that is enzymatically analogous to the original stalled ER4 complex. The ER5* intermediate was needed to accommodate the second, smaller amplitude exponential observed in the kinetic data. Both catalysis and relaxation steps were assumed to be irreversible on the time-scale of these experiments that are detecting changes in fluorescence primarily due to translocation of the 2AP. Therefore, the model included three sets of observables: all ER4 complexes, ER5*, and

ER5, with the relative fluorescence intensities at a ratio of 10:1:0 respectively. The total and baseline fluorescence values were allowed to vary between experiments.

Results

In this work we used the translocation-dependent quenching of 2-aminopurine fluorescence as a biochemical readout of elongation by CVB3 polymerase. Adding CTP to stalled $3D^{pol}$-RNA elongation complexes resulted in a concentration-dependent exponential fluorescence decrease (Figure 3a) from which we could determine the maximal rate, k_{pol}, for a single nucleotide incorporation cycle (Figure 3b). Optimal curve fitting of the raw data required the addition of a second exponential term whose amplitude was about one-tenth that of the main fluorescence change, but whose rate did not titrate with inhibitor concentration; we thus did not factor this term into the inhibition analysis, but did use it to model a final conformational relaxation of the system after translocation. CTP titration experiments done in the presence of non-cognate NTPs revealed GTP to be a classic competitive inhibitor that retained the native k_{pol} rate at high CTP concentrations, but interestingly showed ATP to have significant effects on both k_{pol} and K_m (Figure 3b). In the presence of 4.9 mM ATP, the CTP K_m value increased from 27 ± 6 μM to 41 ± 1 μM and k_{pol} decreased from 22 ± 1.0 s^{-1} to 4.1 ± 0.1 s^{-1}. A preliminary analysis of these data indicated ATP had a low millimolar uncompetitive inhibition constant.

ATP is a Mixed Inhibitor of CVB3 $3D^{pol}$

To better quantitate inhibition of CTP incorporation by non-cognate NTPs, stopped-flow experiments were conducted in which inhibitors were titrated from ≈200 μM to ≈2 mM against three or four constant CTP concentrations ranging from 0.5 to 2.5 times the CTP K_m value. Inverse rates as a function of inhibitor concentration were plotted and analyzed using single-reciprocal Dixon ($1/v$ vs. [Inhibitor]) and Cornish-Bowden ([CTP]/v vs. [Inhibitor]) plots. A series of NTP titrations done at four different fixed CTP concentrations showed a clear point of intersection for GTP on the Dixon plot (Figure 3c), reflecting competitive inhibition with a $K_{ic(GTP)}$ of 440 μM that is comparable to the 300 μM physiological concentration of GTP.[20] The GTP titration lines were parallel in the Cornish-Bowden plot, indicating there was no uncompetitive inhibition term (Figure 3c). A similar analysis of UTP also showed purely competitive inhibition with a $K_{ic(UTP)}$ of 2.9 mM, which is about ten-fold higher than the approximately 250 μM physiological concentration of UTP.[20] Since there was not strong inhibition by UTP, it was not used in subsequent experiments. For ATP, the Dixon plot analysis resulted in a competitive inhibition $K_{ic(ATP)}$ value of 1.5 mM, but in contrast to GTP and UTP, the ATP Cornish-Bowden plot also showed a clear intercept, indicating that ATP is also an uncompetitive inhibitor with a $K_{iu(ATP)}$ of 1.9 mM (Figure 3d). Notably, both $K_{ic(ATP)}$ and $K_{iu(ATP)}$ values are slightly below the estimated physiological ATP concentration of 2.1 mM.[20] Table 1 lists all kinetic parameters with their errors.

ATP Inhibition is Phosphate Dependent

To parse which components of ATP are necessary for its inhibitory effects, titration experiments were performed with ADP and AMP (Figure 4a). Adenosine was not soluble enough for experimental analysis. ADP showed a mixed inhibition profile with competitive

(2.4 mM) and uncompetitive inhibition (4.7 mM) constants that are ≈2-fold reduced compared to the ATP values. AMP had a six-fold weaker competitive component than ATP (10.6 mM) and notably there was no detectable uncompetitive effect. These results indicate that allosteric ATP inhibition depends largely on the triphosphate moiety, especially the β- and γ-phosphates, without which uncompetitive inhibition is essentially abolished.

ATP Uncompetitive Inhibition is Reduced in Motif A Mutants

We next examined ATP and GTP inhibition of two motif A mutant polymerases, I230F and F232Y, that were previously found to have significantly reduced fidelity and increased k_{pol} values.[14] Both mutants had an almost two-fold reduction in the $K_{ic(ATP)}$ value while competitive inhibition by GTP was unaffected (Table 1). However, the $K_{iu(ATP)}$ values were significantly increased (Figure 4b), indicating that ATP uncompetitive inhibition was weakened for F232Y and essentially abolished for I230F.

The side chains of I230 and F232 form the bottom of a pocket on the $3D^{pol}$ surface located below the NTP entry channel and motif D (Figure 5), and this region was identified by CASTp[21,22] as the largest solvent-accessible pocket on CVB3 $3D^{pol}$ outside the active site (data not shown). This led us to hypothesize that the effect of these mutations may be to directly perturb ATP binding at the allosteric site. A closer analysis of this putative binding pocket shows that it is largely composed of peptide backbone groups and is therefore difficult to mutate. However, the surface exposed His228 forms the outer edge of the pocket and due to its minimal interactions with other $3D^{pol}$ residues is a good candidate for mutagenesis that may perturb ligand binding without dramatic effects on local packing. His228 also coordinates a sulfate ion in the CVB3 $3D^{pol}$ structure (PDB 3DDK) suggesting it may act as a counter-ion for the ATP triphosphate moiety. Two mutant polymerases, H228A and H228E, were made and found to be enzymatically active. Both had $K_{ic(ATP)}$ values comparable to that of wild type $3D^{pol}$, but neither had a well-defined $K_{iu(ATP)}$ (Figure 4b, Table 1).

To further assess the importance of this pocket for ATP binding, a less direct M310W mutation was made beneath the pocket (Figure 5b). This would not directly alter the pocket surface, but is likely to cause local rearrangements that would interfere with ATP binding. The M310W polymerase was purified and tested in elongation assays, where it was found to be active and form stable elongation complexes. Its ATP uncompetitive inhibition was attenuated about 2-fold, and there were milder effects on the competitive $K_{ic(GTP)}$ and $K_{ic(ATP)}$ values (Table I). Last, we recently identified F364W in motif D as an attenuating high-fidelity mutation[23] that is also located in this region of the structure where it could also influence $K_{iu(ATP)}$, but this mutant did not deviate significantly from wild type in any of the kinetic parameters (Figure 4, Table 1).

Kinetic Modeling

Our approach to kinetic modeling with KinTek Explorer was to sequentially establish constraints on the model by fitting a series of experiments. The first experiment was an eight-point titration of CTP from 12 to 120 μM with no inhibitors present, yielding k_{pol} and K_m values of 20 ± 2 s^{-1} and 24 ± 9 μM that were in good agreement with values from the

graphical analysis. These values were then fixed for the rest of the global fitting experiments. In the second round, a GTP titration from 200 to 2000 μM against 10 μM CTP was fitted to obtain a $K_{ic(GTP)}$ of 540 ± 80 μM, which was also within error of the value obtained from the Dixon plot. Third, a UTP titration from 200 to 2000 μM yielded a value of 3100 ± 800 μM that was also in good agreement with the Dixon analysis, albeit with a large error since the titration was carried out so far below the $K_{ic(UTP)}$.

Fitting $K_{ic(ATP)}$ and $K_{iu(ATP)}$ required two different experiments and additional assumptions. It was assumed that ATP- and CTP-binding did not affect each other, i.e., the system is effectively noncompetitive and the only effect of allosteric ATP binding was to produce the ER4CA species that had a reduced rate for CTP incorporation as compared to the uninhibited ER4C species. An ATP titration against constant CTP exhibited a well-constrained $K_{ic(ATP)}$ but a poorly constrained $K_{iu(ATP)}$, whereas a CTP titration against a high concentration of ATP was just the reverse. So in the fourth experiment, $K_{ic(ATP)}$ was determined first by a titration of ATP from 200 to 2000 μM against 10 μM CTP without including the uncompetitive pathway. This value was then fixed, and in the fifth experiment the uncompetitive $K_{iu(ATP)}$ term was determined by fitting a CTP titration from 50 to 500 μM in the presence of 4.8 mM ATP. Neither inhibition constant was appreciably different from the graphical analysis results (Table 1), and the globally fitted rate of ER4CA going to ER5* was 5.5 ± 0.2 s^{-1}, reflecting a roughly 4-fold reduction in rate. Last, the second exponential term observed in the kinetic traces, i.e. the non-titrating lower amplitude term, reflects a slow (≈1 s^{-1}) conformation change as the post-translocation ER5* species relaxes to the final ER5 species.

A major advantage of using the kinetic simulation is the ability to judge which parameters are covariant.[18,24] This provides useful information about redundancy in the model and also serves as a test of how well the molecular events in the experimental system are understood. Even minor (≤ 2-fold) changes of the fitted values for the parameters described here caused the model to obviously deviate from the experimental data. Additionally, no two parameters had equivalent effects on the model, nor could the model compensate if any were omitted, which suggests that the mechanism was not over-parameterized with respect to the available data.

Discussion

Unlike other classes of single-subunit polymerases that use swinging motions in the fingers domain to move the incoming nucleotide and templating base into the active site after initial base-pairing, the positive-strand RNA virus RdRPs have a fully prepositioned templating base in the active site and couple nucleotide discrimination with active site closure.[9] This implies that, in the cellular context, all four nucleotides are in direct competition for the active site and that fidelity depends greatly upon the polymerase's sensitivity to the geometry of the nucleotide. Such sensitivity has been shown to be largely mediated by motions of motif A in response to a NTP-induced hydrogen-bond network linking the palm domain to the ribose 2′-hydroxyl group to the fingers domain.[9] As might therefore be expected, motif A mutants that lower fidelity also have a reduced ability to discriminate between CTP and 2′-deoxy-CTP, though they do not significantly alter the apparent affinity

for CTP. This raised the question of whether these mutants only alter the dynamics of active site closure or also increase the affinity of the polymerase for non-cognate nucleotides. The inhibition experiments described here provide a tractable way to directly investigate the effects of fidelity mutants on this affinity.

The measured competitive inhibition constants (K_{ic}) for GTP and ATP roughly scale with their physiological concentrations, whereas the value for UTP is tenfold higher than its estimated cellular concentration. This is somewhat surprising since the templating base in this system is guanine, with which uracil can base-pair better than the purines. The observed lower affinity for UTP is potentially a mechanism whereby the polymerase limits mutations arising from the more readily formed G-U mismatch. It is also interesting that the GTP and ATP K_{ic} values are near their physiological concentrations, indicating that non-cognate nucleotides are by no means excluded from the active site. In the cell these could occupy an appreciable portion of active sites at any given time and the polymerase should have slower kinetics than what is indicated by *in vitro* studies in which only the cognate nucleotide is present.

The initial hypothesis that the previously identified I230F and F232Y fidelity mutants may alter polymerase affinities for non-cognate nucleotides has been largely negated by our data. $K_{ic(GTP)}$ hovers around 400 μM for all CVB3 $3D^{pol}$ mutants (Table 1) while $K_{ic(ATP)}$ varied more broadly, with almost 2-fold decreases for the I230F and F232Y mutants. However, as discussed below, these observed $K_{ic(ATP)}$ values may be influenced by the uncompetitive component of ATP inhibition, making it difficult to establish whether the actual competitive affinity of the active site for ATP is altered by these mutations.

Mechanism of ATP Inhibition

The Dixon and Cornish-Bowden analysis unambiguously identifies ATP as a mixed inhibitor of CVB3 $3D^{pol}$ with an uncompetitive component that indicates ATP binds an allosteric site on the enzyme. Allosteric regulation of nucleic acid polymerases by NTPs is not without precedent. Transcription initiation by *E. coli* RNA polymerase at a T7 A1 promoters has been shown to be allosterically inhibited by UTP.[25] ATP was also found to be a mixed inhibitor of HIV-1 reverse transcriptase elongation.[26] The hepatitis C RdRp, NS5B, is stimulated by high concentrations of GTP,[27] which can bind at a low-affinity site on the thumb domain as seen in a crystal structure of NS5B.[28] Though mutational analysis indicates the GTP binding site seen in the NS5B crystal structure is not responsible for the observed stimulation *in vitro*, the site is important for replication *in vivo*.[29] Additionally, several allosteric inhibitors of NS5B bind near the GTP binding site.[30] We similarly sought to identify the allosteric binding site in CVB3 $3D^{pol}$ via X-ray crystallography and solved five structures of wildtype $3D^{pol}$ co-crystallized with 10 mM ATP in four different conditions. However, none of these structures revealed any new density that could definitively identify ATP in the allosteric binding site (data not shown).

Beyond the implication of allostery, the data give other hints at the mechanism of ATP inhibition. The relatively small ≈400 μM difference between $K_{ic(ATP)}$ and $K_{iu(ATP)}$ values means that their effects on CTP K_m^{app} roughly cancel per the mixed inhibition equation,

$K_m^{app}=K_m\,(1+[I]/K_{ic})/(1+[I]/K_{iu})$. At an ATP concentration of 4900 uM, the CTP K_m^{app} is predicted to be 28 μM, but the hyperbolic plot in Figure 3b shows a much larger than predicted effect with $K_m^{app}=41\pm1\,\mu M$. This may result from the fact that unlike classic mixed inhibition, in which the inhibitor is thought to bind only one site, ATP can bind both in the active site and in an allosteric site, both of which may affect K_{ic}. Not only so, in classic linear mixed inhibition the inhibitor-bound complex is catalytically inactive, but our KinTek Explorer analysis indicates that allosterically bound ATP produces a species that has a ≈4-fold reduced CTP incorporation rate. In this case, K_{ic} and K_{iu} as determined by graphical analysis do not represent true binding constants since the allosteric pathway has flux across it and is not at equilibrium. This may explain why in the I230F and F232Y mutants, in which uncompetitive inhibition was eliminated, the K_{ic} value decreased from 1500 μM to ≈850 μM, a value that might represent the true K_{ic} value for ATP at the active site.

This mechanism is akin to hyperbolic inhibition, so named because the enzymatic rate approaches a non-zero value as inhibitor concentration goes to infinity due to an active enzyme-inhibitor-substrate complex. This causes the single reciprocal plots to look hyperbolic instead of linear at high inhibitor concentrations. However, no such curvature is present in our Dixon and Cornish-Bowden plots, probably because the ATP concentration was only taken as high as ≈2 mM due to practical considerations such as ionic effects from high Mg^{2+} concentration, a desire to stay within physiologically relevant NTP concentration ranges, and polymerase solubility issues. The predicted allosteric site saturation level is only 50–70% and too low to manifest a significant hyperbolic tendency.

Regardless of the precise ATP inhibition mechanism, its mixed profile is important for several reasons. First, the presence of an allosteric site, especially one that is amenable to biochemical assays by virtue of its effect on *in vitro* elongation, can open the door to drug discovery. Second, the $3D^{pol}$ surface pocket (Figure 5) is well positioned as an allosteric control site due to its proximity to the rate-limiting pre-catalysis[31] movement of motif A during active site closure and the observations from both molecular dynamics[32,33] and NMR[34] that motif D dynamics play a role in NTP binding and delivery into the active site. The fact that ATP slows the polymerase is interesting in light of the observation that $3D^{pol}$ speed and fidelity are negatively correlated for a series of Motif A mutants,[14] suggesting that ATP binding may result in a higher fidelity polymerase. This is supported by the observation that ATP uncompetitive inhibition is effectively abolished in the low-fidelity I230F and F232Y motif A mutants, whereas it is at wild-type levels in the high-fidelity F364W motif D mutant. Perhaps sensitivity to ATP levels allows the virus to switch from a high-fidelity mode for the majority of its infection cycle, maximizing the integrity of the genome that is successfully replicating in the host, to a low-fidelity mode as the cell sickens and nucleotide pools are depleted. This final low-fidelity state would produce a burst of mutated genomes that generate the virus variants and a broader quasispecies distribution needed to launch the next infection cycle.

In conclusion, we have shown that ATP is unique among the natural NTPs in that it can function as an allosteric inhibitor of coxsackievirus B3 polymerase. Efficient inhibition requires the presence of both β- and γ-phosphate groups and data from mutant polymerases

suggest the interaction involves a pocket under the NTP entry channel, but definitive proof of ATP binding in this site was not observed after co-crystallization in multiple $3D^{pol}$ crystal forms. These data provide direct evidence that CVB3 $3D^{pol}$ activity can be regulated by a small molecule and raises the possibility that allostery could be used to modulate viral replication fidelity.

Acknowledgments

Funding Sources

This work was funded by NIH award R01 AI059130 to OBP.

We thank Grace Campagnola for assistance with protein purification and stopped flow experiments and Jay Nix for a steady stream of X-rays.

Abbreviations

CVB3	Coxsackievirus B3
$3D^{pol}$	picornaviral RNA-dependent RNA polymerase (RdRP)
K_{ic}	competitive inhibition constant
K_{iu}	uncompetitive inhibition constant

References

1. Rotbart HA. Treatment of picornavirus infections. Antiviral Res. 2002; 53:83–98. [PubMed: 11750935]
2. Whitton JL, Cornell CT, Feuer R. Host and virus determinants of picornavirus pathogenesis and tropism. Nat Rev Microbiol. 2005; 3:765–776. [PubMed: 16205710]
3. Holland BYJJ Ph D, Mclaren LEROYC Ph D, Hoyer BH. Enteroviral Ribonucleic Acid. 1960; 5010:841–864.
4. Emini, Ea, Schleif, Wa, Colonno, RJ., Wimmer, E. Antigenic conservation and divergence between the viral-specific proteins of poliovirus type 1 and various picornaviruses. Virology. 1985; 140:13–20. [PubMed: 2981447]
5. De Palma AM, Vliegen I, De Clercq E, Neyts J. Selective inhibitors of picornavirus replication. Med Res Rev. 2008; 28:823–884. [PubMed: 18381747]
6. Norder H, De Palma AM, Selisko B, Costenaro L, Papageorgiou N, Arnan C, Coutard B, Lantez V, De Lamballerie X, Baronti C, Solà M, Tan J, Neyts J, Canard B, Coll M, Gorbalenya AE, Hilgenfeld R. Picornavirus non-structural proteins as targets for new anti-virals with broad activity. Antiviral Res. 2011; 89:204–218. [PubMed: 21236302]
7. Thompson, Aa, Albertini, Ra, Peersen, OB. Stabilization of Poliovirus Polymerase by NTP Binding and Fingers-Thumb Interactions. J Mol Biol. 2007; 366:1459–1474. [PubMed: 17223130]
8. Ferrer-Orta C, Ferrero D, Verdaguer N. RNA-Dependent RNA Polymerases of Picornaviruses: From the Structure to Regulatory Mechanisms. Viruses. 2015; 7:4438–4460. [PubMed: 26258787]
9. Gong P, Peersen OB. Structural basis for active site closure by the poliovirus RNA-dependent RNA polymerase. Proc Natl Acad Sci U S A. 2010; 107:22505–22510. [PubMed: 21148772]
10. Lauring AS, Frydman J, Andino R. The role of mutational robustness in RNA virus evolution. Nat Rev Microbiol. 2013; 11:327–336. [PubMed: 23524517]
11. Kati WM, Johnson KA, Jerva LF, Anderson KS. Mechanism and fidelity of HIV reverse transcriptase. J Biol Chem. 1992; 267:25988–25997. [PubMed: 1281479]

12. Cornish-Bowden, A. Fundamentals of Enzyme Kinetics. 4. Wiley-Blackwell; 2014. Competition Between Substrates; p. 149
13. Gnadig NF, Beaucourt S, Campagnola G, Borderia aV, Sanz-Ramos M, Gong P, Blanc H, Peersen OB, Vignuzzi M. Coxsackievirus B3 mutator strains are attenuated in vivo. Proc Natl Acad Sci. 2012; 109:E2294–E2303. [PubMed: 22853955]
14. Campagnola G, Mcdonald S, Beaucourt S. Structure-Function Relationships Underlying the Replication Fidelity of Viral RNA-dependent RNA Polymerases. 2014; 89:275–286.
15. Gong P, Campagnola G, Peersen OB. A quantitative stopped-flow fluorescence assay for measuring polymerase elongation rates. Anal Biochem. 2009; 391:45–55. [PubMed: 19406094]
16. Dixon M. The determination of enzyme inhibitor constants. Biochem J. 1953; 55:170–171. [PubMed: 13093635]
17. Cornish-Bowden A. A simple graphical method for determining the inhibition constants of mixed, uncompetitive and non-competitive inhibitors. Biochem J. 1974; 137:143–144. [PubMed: 4206907]
18. Johnson KA, Simpson ZB, Blom T. Global kinetic explorer: a new computer program for dynamic simulation and fitting of kinetic data. Anal Biochem. 2009; 387:20–29. [PubMed: 19154726]
19. Johnson KA, Simpson ZB, Blom T. FitSpace explorer: an algorithm to evaluate multidimensional parameter space in fitting kinetic data. Anal Biochem. 2009; 387:30–41. [PubMed: 19168024]
20. Traut TW. Physiological concentrations of purines and pyrimidines. Mol Cell Biochem. 1994; 140:1–22. [PubMed: 7877593]
21. Binkowski TA. CASTp: Computed Atlas of Surface Topography of proteins. Nucleic Acids Res. 2003; 31:3352–3355. [PubMed: 12824325]
22. Dundas J, Ouyang Z, Tseng J, Binkowski A, Turpaz Y, Liang J. CASTp: computed atlas of surface topography of proteins with structural and topographical mapping of functionally annotated residues. Nucleic Acids Res. 2006; 34:W116–W118. [PubMed: 16844972]
23. McDonald S, Block A, Beaucourt S, Moratorio G, Vignuzzi M, Peersen OB. Design of a Genetically Stable High-Fidelity Coxsackievirus B3 Polymerase That Attenuates Virus Growth in vivo. J Biol Chem. 2016 jbc.M116.726596.
24. Joyce CM. Techniques used to study the DNA polymerase reaction pathway. Biochim Biophys Acta. 2010; 1804:1032–1040. [PubMed: 19665596]
25. Johnson RS, Chester RE. UTP Allosterically Regulates Transcription by Escherichia coli RNA Polymerase from the Bacteriophage T7 A1 Promoter. J Mol Biol. 2002; 318:305–320. [PubMed: 12051839]
26. Yokoyama M, Mori H, Sato H. Allosteric Regulation of HIV-1 Reverse Transcriptase by ATP for Nucleotide Selection. PLoS One. 2010; 5:e8867. [PubMed: 20111609]
27. Lohmann V, Overton H, Bartenschlager R. Selective Stimulation of Hepatitis C Virus and Pestivirus NS5B RNA Polymerase Activity by GTP. J Biol Chem. 1999; 274:10807–10815. [PubMed: 10196156]
28. Bressanelli S, Tomei L, Rey FA, De Francesco R. Structural analysis of the hepatitis C virus RNA polymerase in complex with ribonucleotides. J Virol. 2002; 76:3482–3492. [PubMed: 11884572]
29. Cai Z, Yi M, Zhang C, Luo G. Mutagenesis Analysis of the rGTP-Specific Binding Site of Hepatitis C Virus RNA-Dependent RNA Polymerase. J Virol. 2005; 79:11607–11617. [PubMed: 16140738]
30. Sofia MJ, Chang W, Furman PA, Mosley RT, Ross BS. Nucleoside, nucleotide, and non-nucleoside inhibitors of hepatitis C virus NS5B RNA-dependent RNA-polymerase. J Med Chem. 2012; 55:2481–2531. [PubMed: 22185586]
31. Arnold JJ, Cameron CE. Poliovirus RNA-Dependent RNA Polymerase ($3D^{pol}$): Pre-Steady-State Kinetic Analysis of Ribonucleotide Incorporation in the Presence of Mg 2+ Biochemistry. 2004; 43:5126–5137. [PubMed: 15122878]
32. Moustafa IM, Shen H, Morton B, Colina CM, Cameron CE. Molecular Dynamics Simulations of Viral RNA Polymerases Link Conserved and Correlated Motions of Functional Elements to Fidelity. J Mol Biol. 2011; 410:159–181. [PubMed: 21575642]

33. Shen H, Sun H, Li G. What Is the Role of Motif D in the Nucleotide Incorporation Catalyzed by the RNA-dependent RNA Polymerase from Poliovirus? PLoS Comput Biol (MacKerell, A D., Ed). 2012; 8:e1002851.

34. Yang X, Smidansky ED, Maksimchuk KR, Lum D, Welch JL, Arnold JJ, Cameron CE, Boehr DD. Motif D of viral RNA-dependent RNA polymerases determines efficiency and fidelity of nucleotide addition. Structure. 2012; 20:1519–1527. [PubMed: 22819218]

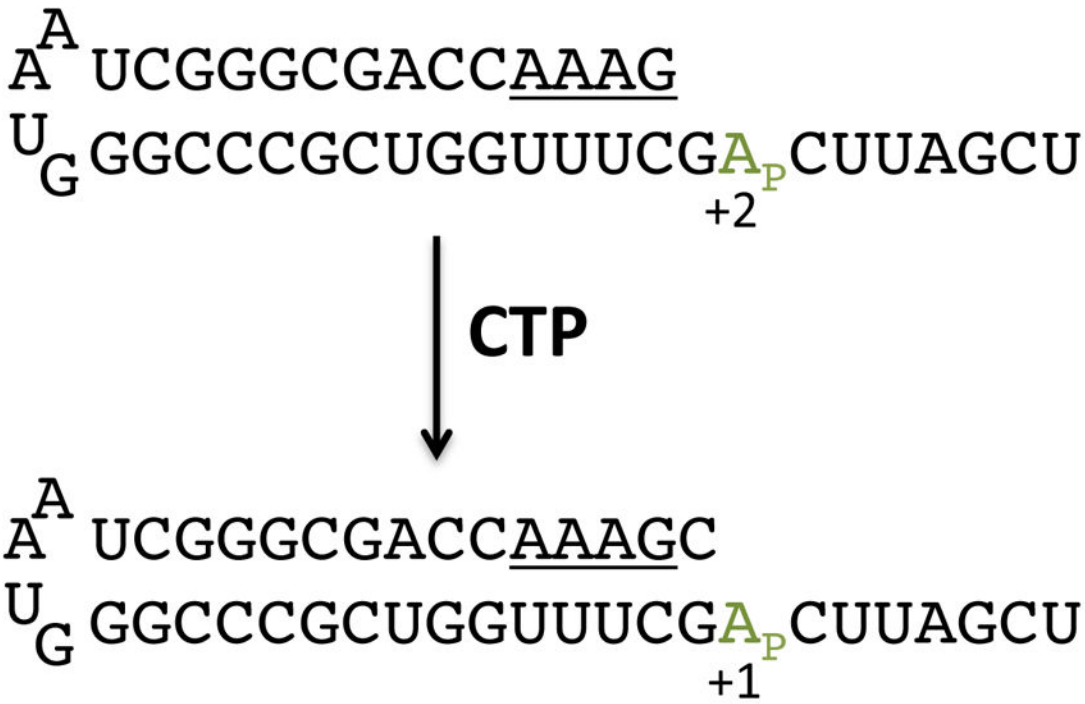

Figure 1.

Schematic of stem-loop RNA used for fluorescence detection of single cycle $3D^{pol}$ elongation. Incorporation of AMP and GMP (underlined) results in a stalled elongation complex that is used in stopped-flow experiments. CMP incorporation plus translocation moves the 2-aminopurine (A_P) from the unstacked +2 position to the partially stacked +1 position, resulting in quenching of fluorescence.

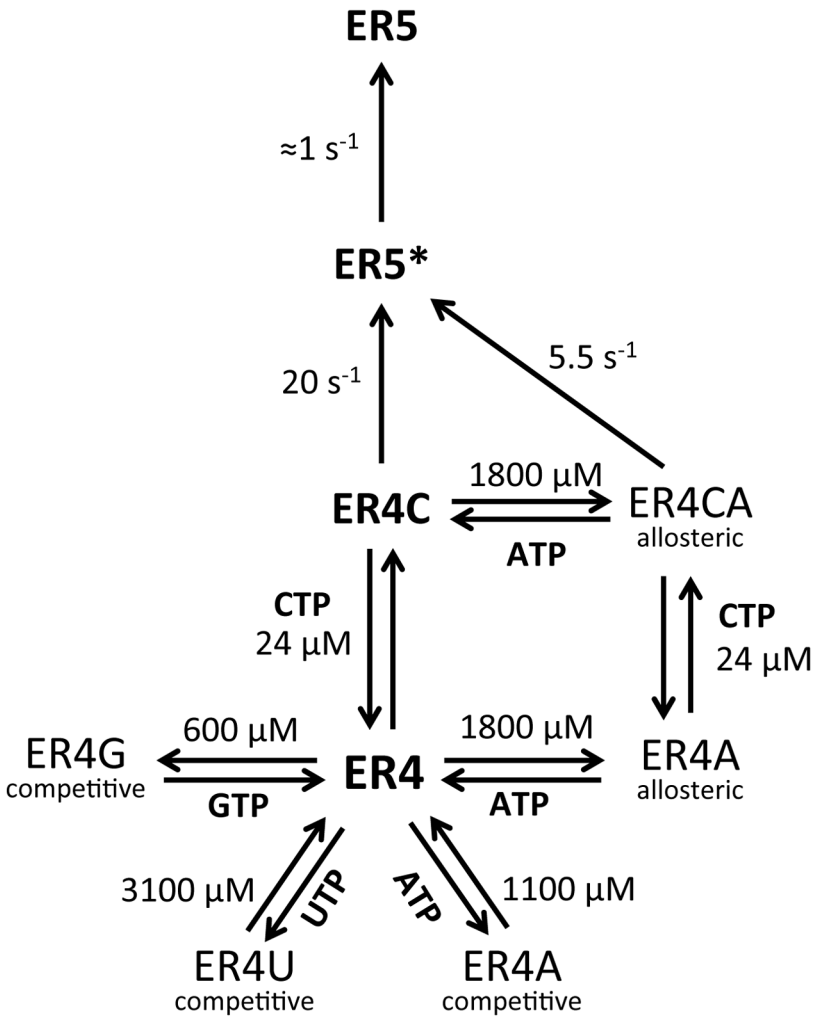

Figure 2.

Global kinetic model for $3D^{pol}$ single step elongation and NTP inhibition. The reaction pathway begins with ER4, the stalled enzyme-RNA complex after four incorporation steps (Figure 1), and models catalysis as a three-step process with CTP binding to form ER4C followed by irreversible incorporation and translocation to yield ER5*, and a final relaxation event to yield ER5. The other nucleotides compete with CTP for the ER4 species. ATP can also bind at an allosteric site, resulting in an $ER4A_{allosteric}$ complex that can bind CTP to form a slowed but catalytically competent ER4CA species. K_m and rate constant values were obtained from global fitting as described in the results, with errors listed in Table 1.

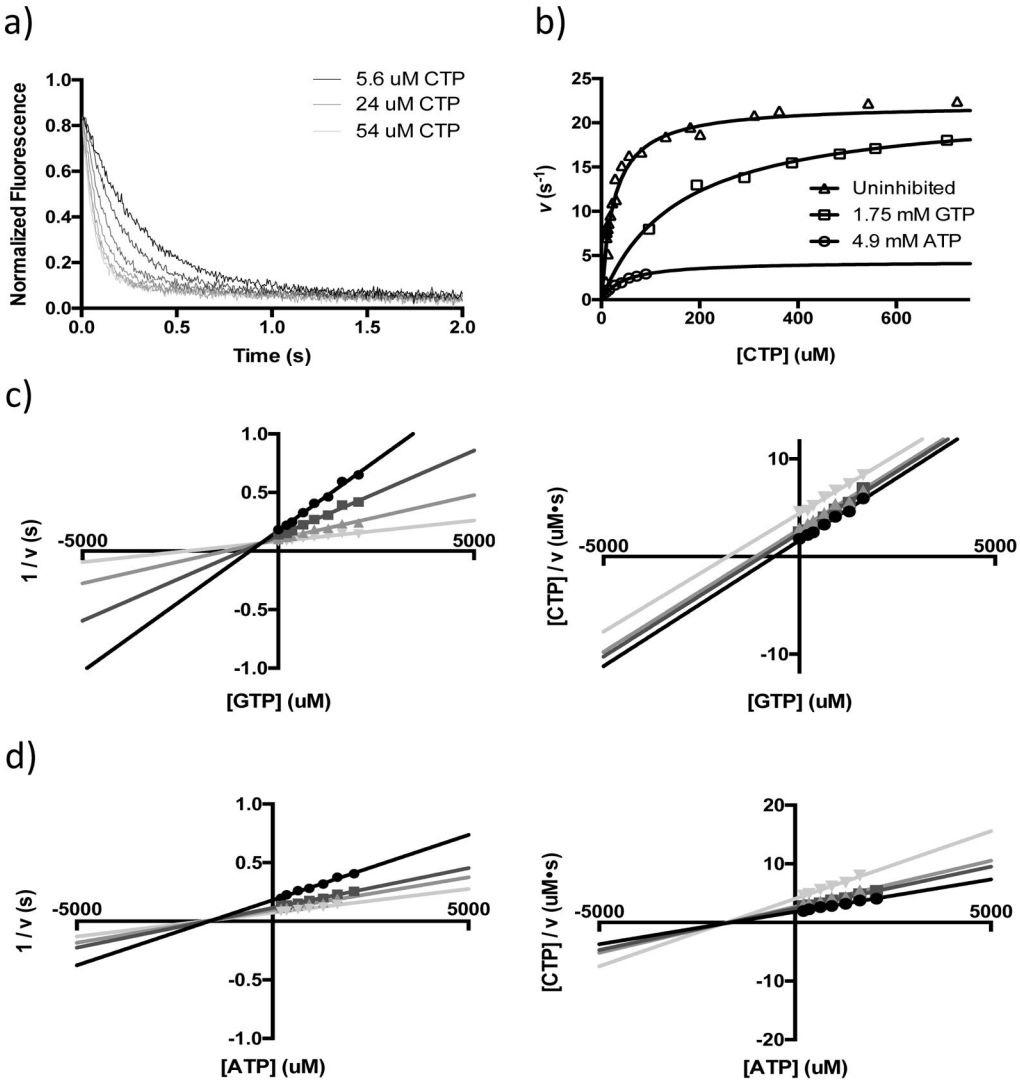

Figure 3.

Inhibition of $3D^{pol}$ elongation cycle by ATP and GTP. (a) Representative stopped-flow traces from a CTP titration experiment. (b) Representative hyperbolic plots from which V_{max} and K_m values were derived. (c–d) Dixon (left) and Cornish-Bowden (right) plots of data from (c) GTP and (d) ATP titrations done at four different CTP concentrations ranging from 10 μM (black) to 56 μM (pale grey). Lines represent a simultaneous best-fit of all the data where the curves were forced to share a common intersection point when appropriate.

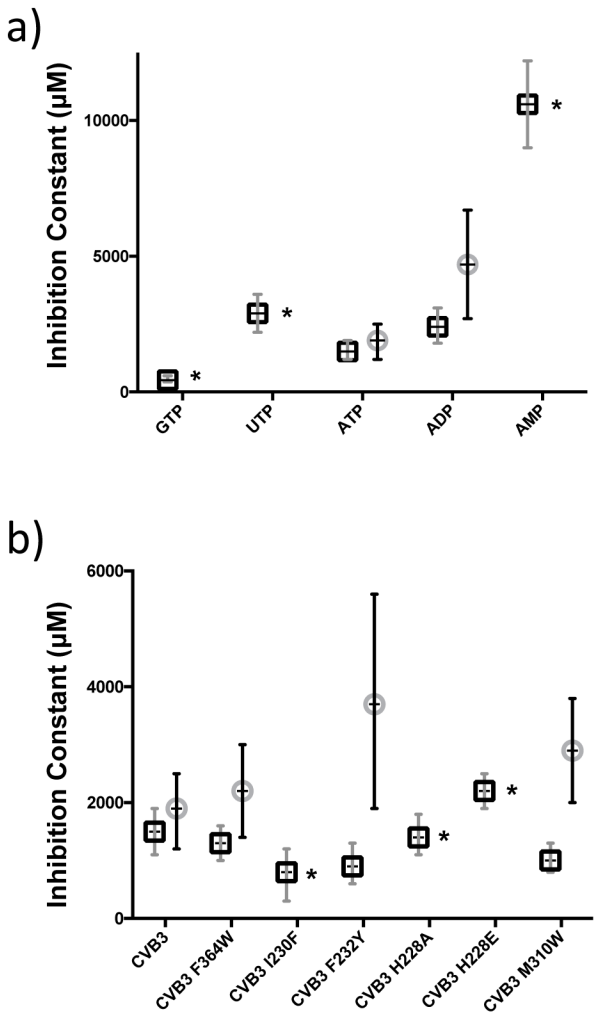

Figure 4.

Analysis of nucleotide and 3D^{pol} features needed for inhibition. Plots show competitive (K_{ic} □) and uncompetitive (K_{iu} ○, * = not observed) inhibition constants with asymmetric error bars representing the 95% confidence intervals from curve fitting. a) Among native NTPs, only ATP shows uncompetitive inhibition, which is dependent on both beta and gamma phosphates. b) Uncompetitive ATP inhibition is reduced or eliminated by two low-fidelity 3D^{pol} mutations in motif A, I230F and F232Y, and by mutating His228 to alanine and glutamate.

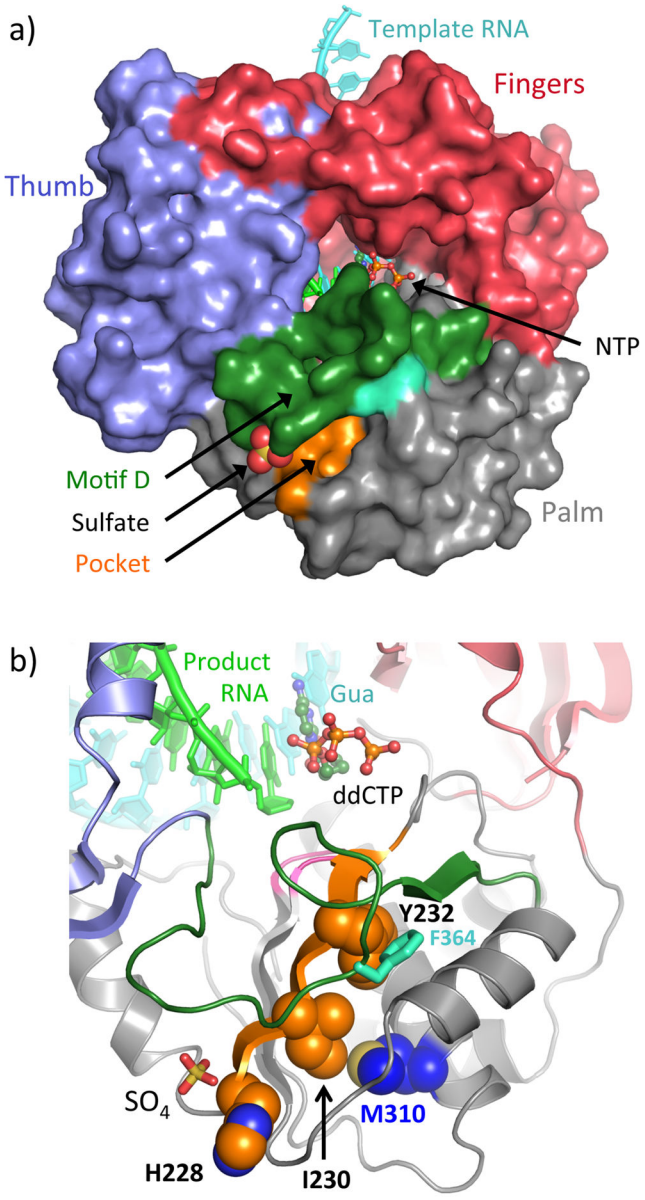

Figure 5.

Putative regulator binding pocket on CVB3 3D^{pol} based on loss of allosteric regulation by ATP in H228A/E, I230F, and F232Y mutants. A) Structure of the stalled CVB3 3D^{pol} elongation complex (PDB:4K4Y) with a bound sulfate from the apo-3D^{pol} structure (PDB: 3DDK). Motif A residues lining the putative allosteric pocket are colored orange, motif D is colored dark green, and Phe364 is marked in lighter green. B) Detailed view of the mutated residues and their location relative to the active site with a bound dideoxy-CTP. Mutated motif A residues are shown as orange spheres and Phe364 in motif D is shown in light green sticks.

Table 1

Nucleotide Inhibition Parameters for CVB3 $3D^{pol}$.

	Global[a]	Graphical[b]						
	Wild Type	**Wild Type**	**F364W**	**I230F**	**F232Y**	**H228A**	**H228E**	**M310W**
$K_{ic(GTP)}$	590 ± 80	440 ± 60	490 ± 60	360 ± 80	460 ± 80	380 ± 90	350 ± 80	350 ± 75
$K_{ic(UTP)}$	3100 ± 800	2900 ± 300	n.d.[c]	n.d.	n.d.	n.d.	n.d.	n.d.
$K_{ic(ATP)}$	1100 ± 200	1500 ± 200	1300 ± 100	800 ± 200	900 ± 200	1400 ± 200	1900 ± 300	1000 ± 110
$K_{iu(ATP)}$	1800 ± 100	1900 ± 300	2200 ± 400	n.a.[d]	3700 ± 900	n.a.	3900 ± 1000	2900 ± 400

All units are μM.

[a] Global fitting with *KinTek Explorer* software with standard errors.

[b] Graphical analysis via Dixon and Cornish-Bowden plots with standard error of the fitted parameters.

[c] n.d. = UTP inhibition constants were not determined for the mutant polymerases.

[d] n.a. = uncompetitive inhibition was not observed.